7B.8 SURFACE BIDIRECTIONAL REFLECTANCE FUNCTIONS DERIVED FROM CERES HELICOPTER DATA OVER THE ARM SOUTHERN GREAT PLAINS SITE

Shalini Mayor*, David R. Doelling, Mandana M. Khaiyer
Analytical Services and Materials, Inc.
Hampton, Virginia

Patrick Minnis and Donald R. Cahoon, Jr.
Atmospheric Sciences Research, NASA Langley Research Center
Hampton, Virginia

1. INTRODUCTION

Bidirectional reflectance distribution functions (BRDFs) are essential for deriving albedos from radiances measured by satellites to estimate the observed global energy balance and for predicting the radiance field for a given set of conditions. BRDFs were derived from data taken by the helicopter-based Clouds and the Earth's Radiant Energy System (CERES) Airborne Radiometer Scanner (ARS; Wheeler et al. 1997) system over a variety of surface types around the Atmospheric Radiation Measurement (ARM) Southern Great Plains (SGP) site during August 1998. Data were taken at low altitudes for solar zenith angles ranging from 23° to 90°. The ARS contains the FieldSpec FR spectroradiometer with spectral sampling from 0.35 to 2.5 μm. The BRDFs were computed using clear-sky data in spectral intervals corresponding to channels on several new satellite imagers. The results are compared for variability with wavelength and surface type. The reflectances were corrected to the top of the atmosphere (TOA) for use with satellite data. These results should help improve the accuracy of satellite-derived cloud and surface radiative properties.

2. DATA

The CERES ARS system consists of a self-navigating Bell UH-1H helicopter-based scanner system which allows precise measurement of surface BRDFs. The FieldSpec FR spectroradiometer, built by Analytical Spectral Devices provides nearly continuous spectral sampling from 0.35 to 2.5 μm in 3 to 12-nm intervals. During bidirectional operations, the starboard pod (containing the FieldSpec FR) rotates along the pitch plane in order to track ground targets as shown in Fig. 1.

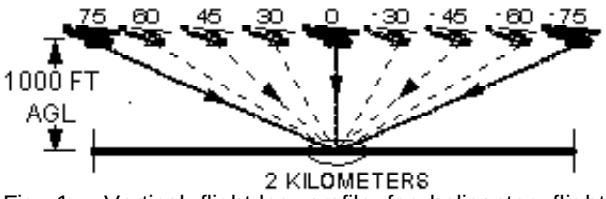

Fig. 1. Vertical flight-leg profile for helicopter flight pattern.

As the ARS passes over the ground target, the starboard pod maintains a constant fix, thus providing continuous measurements from +75° to -75° relative to nadir. Five leg patterns are flown, as shown in Fig. 2, to allow 10 separate azimuthal measurements over the target. Bidirectional measurements have been taken over a variety of vegetation types (e.g., fallow wheat, grass, milo, and soybeans) around the SGP Cloud and Radiation Testbed (CART) site.

3. METHODOLOGY

To describe the angular variation of radiance, the angular coordinates were divided into ranges, or angular bins, and the model is represented by

*Corresponding author address: Patrick Minnis, NASA Langley Research Center, MS 420, Hampton, VA 23681-2199. email: p.minnis@larc.nasa.gov.

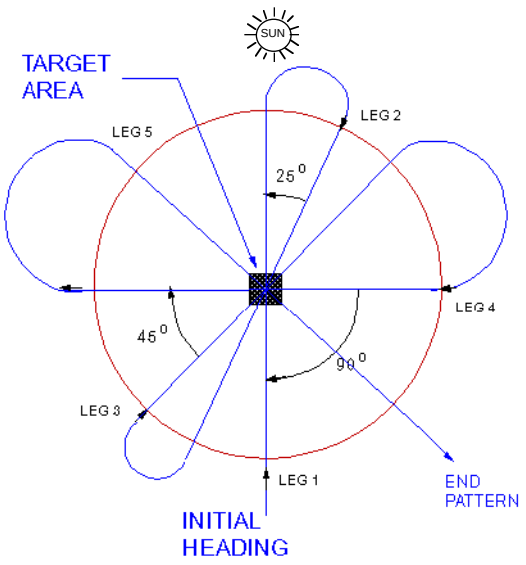

Fig. 2. CERES ARS typical BRDF pattern (overhead view).

the mean values for each bin. These bins are defined by increments of 10° viewing zenith angle (VZA), 10° solar zenith angle (SZA) and, relative azimuths centered at 6°, 25°, 45°, 90°, 135°, 155°, 174°. Data from all vegetation types were averaged into these bins.

To apply the model to satellite data, the reflectances derived from the helicopter data were corrected to the TOA by accounting for molecular scattering and ozone absorption for the visible channel (0.65μm). The correction for ozone absorption and Rayleigh scattering follow the procedures of Minnis et al. (1993). The reflectance parameterization is described below.

The reflectance at the TOA is

$$\rho_{toa} = t_{\mu}\left[\rho_{ray}\left(\mu_0,\mu,\psi\right) + \rho_{Fspec}\left(\mu_0,\mu,\psi\right)\right] \qquad (1)$$

where t_μ is the upward transmittance and ρ_{ray} is the reflectance of the overlying Rayleigh layer. The reflectance at the helicopter, ρ_{Fspec}, is defined as

$$\rho_{Fspec} = \frac{R_{meas}}{E_{\lambda}\left(1-\alpha_{ray}\right)t_{a1}} \qquad (2)$$

where α_{ray} is the albedo of Rayleigh layer above the helicopter, E_λ is the spectral solar constant (value used in this analysis for 0.65μm channel is 1442.27 $Wm^{-2}\mu m^{-1}$), R_{meas} is the radiance measurement at flight level, t_{a1} is the transmittance of ozone above the helicopter, μ is cos(SZA), μ_o is cos(VZA), and the relative azimuth angle is ψ. For this analysis, the ozone absorption optical depth for the visible channel is fixed at 0.027, a value that corresponds to an ozone path length of 0.35 cm-STP.

For the near-IR channel (1.65 μm), the helicopter-derived reflectances were corrected to the top of atmosphere by accounting for atmospheric absorption above the helicopter with E_λ = 215.34 $Wm^{-2}\mu m^{-1}$ using the method of Sun-Mack et al. (1999).

Due to the limited flight patterns, the time of year (August 1998) and the latitude, not all VZA and SZA bins were filled for the two channels. The most serious problem was values missing for entire SZA bins. To fill some of the empty bins, the Helmholtz Principle of Reciprocity,

$$\mu_o L(\mu_o,\psi;\mu) = \mu L(\mu,\psi;\mu_o),$$

where L is the radiance, was applied first. For reciprocal bins with data, the difference between the observed and predicted radiances (Fig. 3) is unbiased with a root-mean-square difference of 18.7% for 0.65-μm channel, indicating that the use of this principle here is justified. Similar results were obtained for the 1.65-μm channel. Much of the scatter is probably due to the variations in the observed scenes, differing aerosol amounts and humidity for the different days when the helicopter

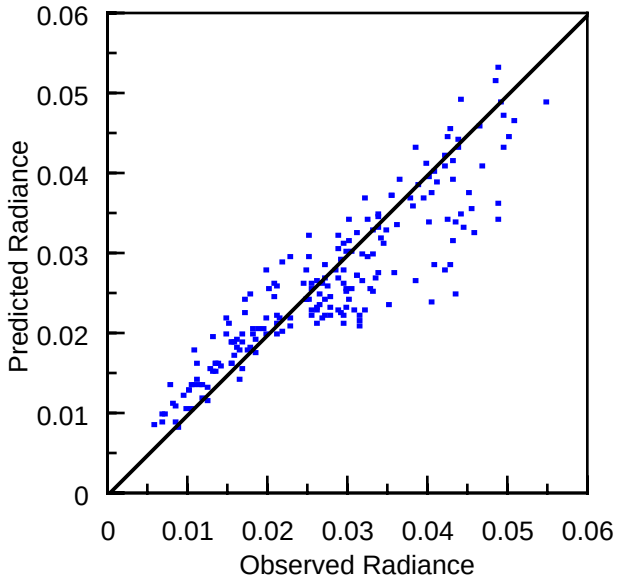

Fig. 3. Application of reciprocity to filled angular bins yielded a rms of 18.7% with bias = 0.001 (Visible channel radiance is $Wm^{-2}sr^{-1}nm^{-1}$).

was deployed for the various solar zenith angles, and variations in the helicopter flight attitude.

To complete each vegetation reflectance model, the missing radiances were filled using extrapolation (second degree polynomial fits) and interpolation techniques.

The corrected radiances in the completed angular bins were then averaged over the various field types.

$$\sum_{sz,vz,az} \frac{\sum_{type=1}^{4} \mu_{0_{type}} L_{type}}{\sum_{type=1}^{4} \mu_{0_{type}}}$$

4. RESULTS

The helicopter data were used to generate reflectances at the instrument altitude and at the TOA. The helicopter flight patterns provided very good coverage for most viewing and all azimuth angles but had limited coverage for solar zenith angles, especially the first two and final solar zenith angle bins which had to be completely filled using external techniques. The helicopter reflectances for 0.65 μm were computed at the TOA by applying (1) and (2). These corrections increased the reflectances by about 5% overall. Atmospheric absorption corrections applied to 1.65-μm channel reflectances to convert to the TOA decreased the values by about 5%. Finally, the TOA reflectances for both channels were integrated over all angles and normalized to create the BRDF models. Figures 4 and 5 show the combined helicopter-measured reflectances from all the vegetation fields at flight level and TOA for an SZA of 45°. For this example, there were no missing bins. At other SZAs, a combination of reciprocity, interpolation and extrapolation was applied to fill missing VZA bins.

In general, the anisotropic factors have small variations over the first 3 SZA bins (not shown), but significant increases in the forward and back scattering peaks are observed at higher solar zenith angles. Figures 6 and 7 compare the helicopter-derived (0.65 μm) and GOES BRDFs (MH; Minnis and Harrison, 1984) for SZA = 55° and 75°, respectively. The major features of the two models are similar. Overall, the helicopter BRDFs show more structure than the MH models. The MH models are most likely smoother because they are taken over a wide variety of land regions while the helicopter data were limited to the ARM SGP region and contain estimates for some bins. Unlike the helicopter models, the MH models were not explicitly corrected to the TOA. Both models become more anisotropic with increasing SZA. The models also show a strong backscattering peak near the anti-solar point and a minimum near nadir in the forward scattering direction.

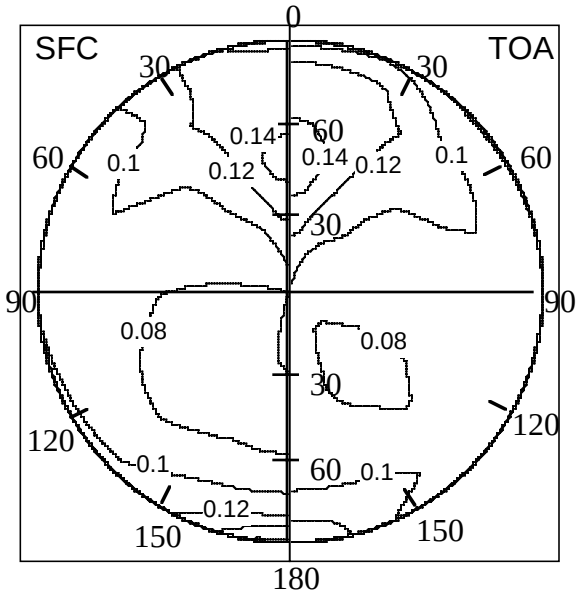

Fig. 4. Comparison of visible reflectances (0.65 μm) derived from helicopter measurements over SGP at the helicopter altitude (SFC) and TOA at SZA=45°.

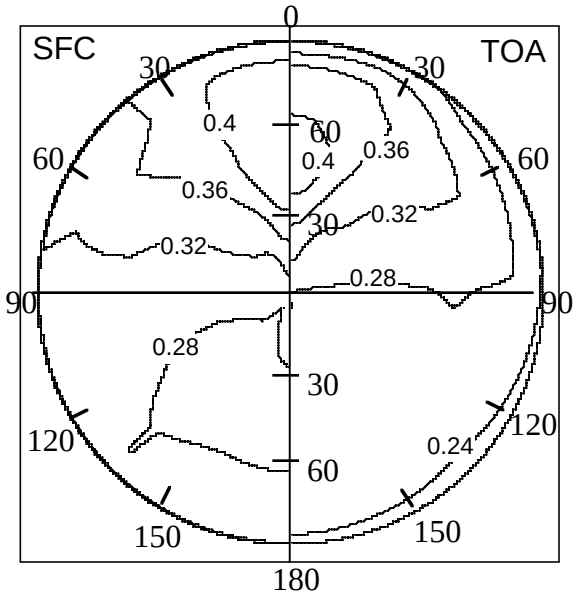

Fig. 5. Same as Fig. 4, except for near-IR reflectance (1.65μm).

The helicopter model will be tested using simultaneous visible channel observations from multiple GOES and Sun-synchronous satellites. Reflectance from a scene observed by one satellite is used with the BRDF model to predict the

reflectance for the other satellite. This approach to estimating the model errors is currently underway.

5. CONCLUDING REMARKS

The helicopter-based BRDF model should improve the accuracy of ARM satellite-derived cloud and radiation products over the SGP area because it was derived from data taken over land representative of the SGP area. Despite its limited coverage, the major features of the model compared reasonably well with the MH BRDFs. Because of its low operating costs, the helicopter-based measurements can provide BRDFs useful for satellite data interpretation. The process of filling missing angular bins increases the uncertainty in the final BRDF model. Hence, data from additional clear-sky helicopter flights are needed to fill more bins and reduce dependence on auxiliary bin filling techniques. Inclusion of aerosols in the correction atmospheric effects should improve the accuracy of the resulting TOA bidirectional distribution functions.

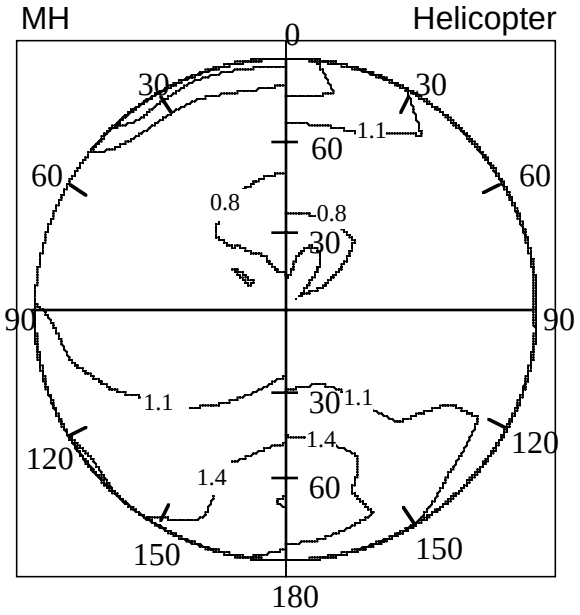

Fig. 6. Comparison of anisotropic visible reflectance factors derived from helicopter measurements (0.65μm) at TOA over SGP and MH BRDF (SZA = 55°).

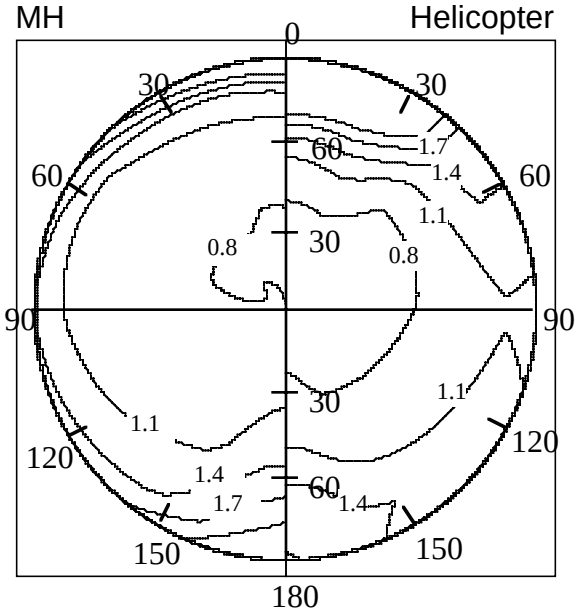

Fig. 7. Same as Fig. 6, except SZA = 75°.

References

Wheeler, R. J., G. C. Purgold, and C. H. Whitlock, 1997: The CERES Airborne Radiometer Scanner. 9th Conference on Atmospheric Radiation, 2-7 February, Long Beach, CA.

Minnis, P. and E. F. Harrison, 1984: Diurnal variability of regional cloud and clear-sky radiative parameters derived from GOES data; Part I: Analysis Method, J. Climate Appl. Meteor., **23**, 993-1011.

Minnis, P., K. Liou and Y. Takano, 1993: Inference of cirrus cloud properties using satellite-observed visible and infrared radiances. I - Parameterization of radiance fields, J. Atmos. Sci., **50**, 1279-1304.

Sun-Mack, S., Y. Chen, T. D. Murray, P. Minnis, and D. F. Young, 1999: Visible clear-sky and near-infrared surface albedos derived from VIRS data for CERES. Proc. AMS 10th Conf. Atmos. Rad., Madison, WI, June 28-July 2.

Acknowledgments

This research was supported by DE-AI02-97ER62341 as part of the ARM Science Team and by the NASA Clouds and the Earth's Radiant Energy System Project. The helicopter data were provided by Mark Wilson of AS&M, Inc.